Received 21 June 2024; revised 17 July 2024; accepted 18 July 2024. Date of publication 26 July 2024;
date of current version 31 July 2024. The review of this article was arranged by Associate Editor Xiaoqing Song.

*Digital Object Identifier 10.1109/OJPEL.2024.3432989*

# Compact Two-Phase Immersion Cooling With Dielectric Fluid for PCB-Based Power Electronics

**ALEKSANDAR RISTIC-SMITH AND DANIEL J. ROGERS (Senior Member, IEEE)**

Department of Engineering Science, University of Oxford, OX1 3PJ Oxford, U.K.

CORRESPONDING AUTHOR: ALEKSANDAR RISTIC-SMITH (e-mail: aleksandar.ristic-smith@eng.ox.ac.uk)

This work was supported in part by U.K. EPSRC and in part by YASA Ltd under grant EP/R513295/1.

**ABSTRACT** This paper explores two-phase immersion cooling using sealed enclosures of dielectric fluid as a technique to achieve compact, power dense converters on a single printed circuit board (PCB). The proposed approach employs passive circulation of the fluid and does not introduce system complexity beyond a heat exchanger required to condense the vapour. A test apparatus representing six 650 V, 150 A semiconductor switches in an inverter rejecting heat to a 65 °C water cooling loop is developed. Pool boiling experiments on a flat surface in Novec 7000 dielectric fluid demonstrate critical heat flux of 43 W cm$^{-2}$ at a saturation temperature of 94 °C and a corresponding pressure of 593 kPa. By augmenting the surface with pin fins (representative of a heat spreader attached to a switch) and grit blasting to improve the surface micro-geometry, the maximum heat transfer coefficient increased from 1.5 W cm$^{-2}$ K$^{-1}$ to 3.4 W cm$^{-2}$ K$^{-1}$ with a corresponding reduction in switch temperature from 125 °C to 107 °C at the total power dissipation of 186 W. A practical implementation with comparable thermal performance to the experimental apparatus but minimised volume of 0.12 L is presented. This yields a Cooling System Performance Index of 37 WL$^{-1}$ K$^{-1}$, including the heat exchanger and printed circuit board with switches, decoupling capacitors and gate drivers.

**INDEX TERMS** Immersion cooling, two-phase cooling, dielectric fluid, power density.

## NOMENCLATURE

*Variables*

- $Q$ Power dissipation [W].
- $q$ Heat flux [W cm$^{-2}$].
- $h$ Heat transfer coefficient [W cm$^{-2}$ K$^{-1}$].
- $T$ Temperature [°C].
- $P$ Pressure [Pa].
- $A$ Area [cm$^2$].
- $x$ Distance along fin [m].
- $t_f$ Fin width [m].
- $L$ Fin length [m].
- $\rho$ Density [kg m$^{-3}$].
- $l_{lv}$ Latent heat [J kg$^{-1}$].
- $c_p$ Specific heat capacity [J kg$^{-1}$ K$^{-1}$].
- $g$ Acceleration due to gravity [ms$^{-2}$].
- $\sigma$ Surface tension [N m$^{-1}$].
- $k$ Thermal conductivity [W m$^{-1}$ K$^{-1}$].
- $\mu$ Dynamic viscosity [Pas].

*Subscripts*

- chf Critical heat flux.
- l Liquid property.
- v Vapour property.
- sw Switch, switch-level.
- sat Property of saturated fluid.

## I. INTRODUCTION

It would be beneficial if highly integrated, compact, low-inductance printed circuit board (PCB) based converters could achieve the excellent thermal performance and high power densities offered by power modules. This could be enabled by a range of novel electronics cooling techniques detailed in literature, including microchannel flow and jet impingement [1]. In [2], it is proposed the metallised ceramic substrate of a

© 2024 The Authors. This work is licensed under a Creative Commons Attribution 4.0 License. For more information, see https://creativecommons.org/licenses/by/4.0/

power module can be removed by employing dielectric fluid cooling in close proximity to semiconductor switches to provide electrical isolation. Through application of single-phase jets impinging on a heat spreader soldered to the switch, a switch-level heat flux of 716 W cm$^{-2}$ was achieved. In [3], semiconductor die are interconnected by a copper lead frame structure and cooled via two-phase flow of Novec 7500 dielectric fluid. Calculations indicate the proposed package reduces volume by 60% and increases heat dissipation by 100% compared with a conventional power module.

Microchannel cooling leverages the increase in heat transfer coefficient with decreasing cooling channel size. This is demonstrated in [4]. A coldplate with 1 mm square channels and two-phase flow of dielectric fluid demonstrated reduction in thermal resistance by 2.4 times compared with a conventional power module water coldplate. An additively manufactured aluminium microchannel heatsink for power semiconductor switches was presented in [5]. Simulations indicate it could sustain switch-level heat fluxes of 521 W cm$^{-2}$ with single-phase flow of Novec 7500 dielectric fluid.

Despite the excellent thermal performance of the aforementioned approaches, system complexity and volume are increased due to pumps, plumbing and heat exchangers required to facilitate flow of dielectric fluids. By contrast, immersion cooling submerges electronic components in a static liquid pool and utilises passive fluid circulation by natural convection or phase change. Two-phase immersion in Galden HT55 dielectric fluid was proposed in [6] for high performance computing chips attached to heat spreaders with thermal interface material. The highest die-level heat flux sustained by boiling was 200 W cm$^{-2}$. In [7], pulse generators based on SOT-23 package transistors were immersed in dielectric fluids undergoing phase change. Superior cooling with FC72 fluid enabled a pulse repetition rate double that achieved with single-phase oil immersion and triple that observed with forced air cooling. A proposed approach to immersion of PCB-based power electronics uses water as the cooling medium [8]. This is achieved by coating all board surfaces and components with electrically isolating Parylene-C. An exceptional switch-level heat flux of 562 W cm$^{-2}$ was reported with coating thickness of 1 $\mu$m. However, since the breakdown voltage of Parylene-C is only 78 V $\mu$m$^{-1}$, this approach is only suited to low-voltage applications.

In this paper, we propose immersion of entire PCB converters in a closed, static pool of dielectric fluid undergoing liquid to vapour phase change. All electronic components are directly cooled by closed-cycle boiling and condensation of the fluid, which also provides electrical isolation to the converter package. At a system level, two-phase immersion cooling requires a single heat exchanger which condenses the vapour and facilitates passive liquid return to the pool.

### A. BOILING HEAT TRANSFER

The envisioned application, depicted in Fig. 1, is a semiconductor switch with planar area $A_{sw}$, immersed in dielectric fluid undergoing phase change from liquid to vapour. Prior work on two-phase immersion for electronics cooling has focused on characterising boiling heat transfer for flat switch surfaces at atmospheric pressure where the fluid pool is maintained at a constant saturation temperature $T_{sat}$ corresponding to the atmospheric pressure boiling point. This is often achieved via an open fluid pool which releases vapour to atmosphere as shown in Fig. 1(a). $T_{sw}$ represents the switch surface temperature in response to power dissipation $Q_{sw}$. The critical heat flux (CHF) represents a practical maximum power per unit switch area:

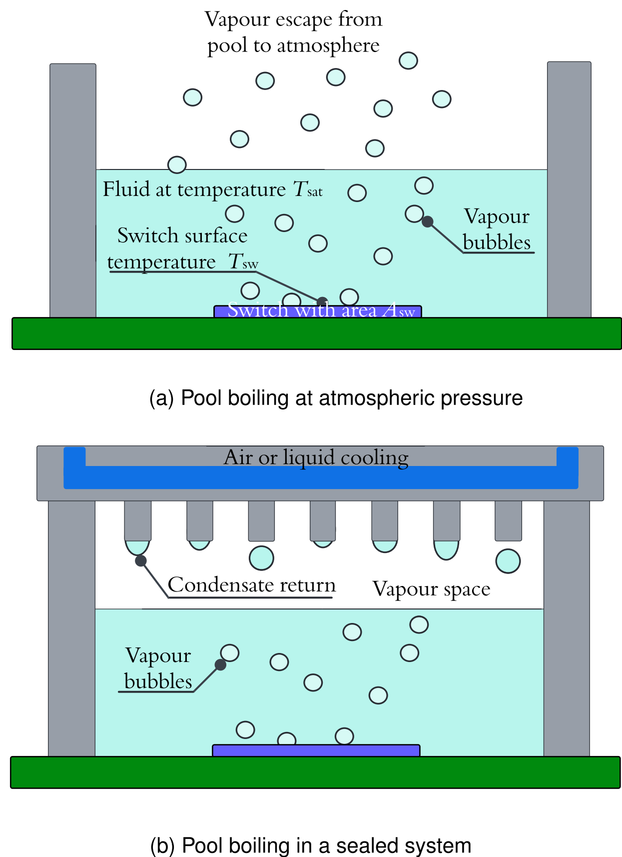


**FIGURE 1.** Semiconductor switches immersed in dielectric fluid.

$$q_{chf} = \frac{\max(Q_{sw})}{A_{sw}} = \max(q_{sw}) \quad (1)$$

One hypothesis states that CHF originates from hydrodynamic aspects of the boiling process [9]. Its significance can be understood by considering the boiling curve, which describes the relationship between heat flux and temperature rise of the switch surface above the fluid saturation temperature. Fig. 2 shows a boiling curve for water at atmospheric pressure.

- In region **(i)**, the switch surface is not hot enough to create vapour bubbles so heat is transferred through convection.
- During nucleate boiling (region **(ii)**), bubbles periodically form, grow and detach from cavities in the switch surface.

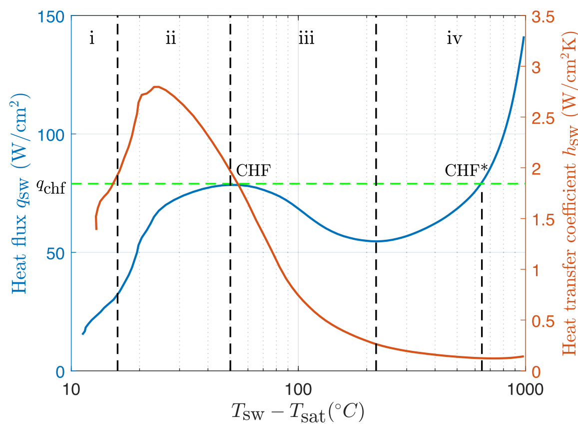


**FIGURE 2. Boiling curve and corresponding heat transfer coefficients for water at atmospheric pressure. Based on data published in [10].**

- At CHF, vapour starts to blanket the surface, impeding heat transfer from the switch to the surrounding liquid.
- In region **(iii)**, vapour covers an increasing portion of the switch surface until a stable film forms in region **(iv)**.

If the power dissipation of an electronic component just exceeds the critical heat flux (point CHF in Fig. 2), a sudden and drastic increase in temperature occurs until steady state is reached in region **(iv)** at point CHF*. In practice, this would cause thermal failure and so point CHF presents a limit on power dissipation.

The heat transfer coefficient defined in (2) is a measure of the heat flux sustained per degree of temperature rise from the fluid to the switch surface in W cm$^{-2}$ K$^{-1}$. For a given heat flux, higher heat transfer coefficient corresponds to a lower switch temperature. For boiling, the heat transfer coefficient is not constant but depends on both $T_{\mathrm{sw}}$ and $T_{\mathrm{sat}}$:

$$h_{\mathrm{sw}} = \frac{q_{\mathrm{sw}}}{(T_{\mathrm{sw}} - T_{\mathrm{sat}})} \tag{2}$$

To maximise converter power density, it is advantageous to increase the peak nucleate boiling heat transfer coefficient in region **(ii)** and the critical heat flux.

Dielectric fluids like Fluorinerts and Novecs from 3 M are commonly used for two-phase immersion cooling due to their widespread chemical compatibility and electrical isolation capability. Studies with Fluorinert FC72 [11], Novec 7000 [12] and Novec 649 [13] indicate these fluids reach CHF around 20 W cm$^{-2}$ on smooth, flat surfaces at atmospheric pressure, with peak heat transfer coefficients below 1 W cm$^{-2}$ K$^{-1}$. Moderate improvements in both criteria are observed by modifying the surface geometry, creating more micro-scale features from which vapour bubbles can nucleate [14]. By treating smooth copper surfaces with emery paper of different grit counts, surface roughness was varied from 0.039 $\mu$m to 0.58 $\mu$m with an accompanying increase in critical heat flux for Novec 7000 from 21.6 W cm$^{-2}$ to 30 W cm$^{-2}$ [12]. Sandblasting was employed in [15] to prepare copper surfaces with roughness up to 9 $\mu$m. Reported heat transfer coefficient and critical heat flux were respectively 3 and 1.5 times higher than the smooth surface.

Further improvements in heat transfer coefficient and CHF are achieved by attaching heat spreaders to semiconductor switches. The heat spreader increases the surface area in contact with fluid and enables higher power dissipation for a given switch [16]. The *switch-level* CHF and heat transfer coefficient, calculated via (1) and (2) with reference to the planar switch area $A_{\mathrm{sw}}$, are therefore improved. There are several proposed mechanisms by which heat spreaders can be coupled to switches, including etching directly into the semiconductor material [17], or press fitting by mechanical force [18]. However, most prior research has focused on characterisating metal heat spreaders which offer higher thermal conductivity than silicon and can be soldered or sintered to switches. In [11] a copper heat spreader with normally protruding, low profile fins of length 0.5 mm yielded switch-level CHF of 51 W cm$^{-2}$ for FC72. This was further increased to 105 W cm$^{-2}$ using a single protruding fin of length 12.7 mm with low profile fins cut into its perimeter [19].

Microporous structures have also been explored as heat spreaders. In addition to increasing heat transfer area, the pores promote fluid circulation in proximity to the switch surface via capillary action. The heat transfer coefficient for Novec 649 was increased from 0.35 W cm$^{-2}$ K$^{-1}$ for a smooth surface to 1.1 W cm$^{-2}$ K$^{-1}$ using a commercial microporous coating [20]. In [21], porous structures with pores aligned in the through plane are attached to grooved copper heat spreaders, separating vapour release and liquid replenishment routes to the switch surface. The reported critical heat flux for FC72 was 75 W cm$^{-2}$ with a maximum heat transfer coefficient of 3.6 W cm$^{-2}$ K$^{-1}$.

More drastic improvements are achieved using heat spreaders with larger planar area than the semiconductor switch. This was demonstrated by attaching a microporous coated finned heat spreader to switches of varying size; the highest switch-level heat transfer coefficient of 15 W cm$^{-2}$ K$^{-1}$ was reported for the smallest switch [16]. Flat heat spreaders with microporous coatings and nine times greater area than the semiconductor switch were characterised in [22]. A maximum switch-level heat transfer coefficient of 12 W cm$^{-2}$ K$^{-1}$ was reported and critical heat flux of 400 W cm$^{-2}$ for Novec 7000 fluid. To the authors' knowledge, the highest reported switch-level critical heat flux and heat transfer coefficient for a boiling dielectric fluid are 1180 W cm$^{-2}$ and 25 W cm$^{-2}$ K$^{-1}$ [23] achieved by soldering both sides of a switch to flat heat spreaders with ten times the area. However, such high switch-level thermal performance requires heat spreaders which extend horizontally and vertically beyond the switch surface and therefore comes with the penalty of increased converter volume.

### B. TWO-PHASE IMMERSION COOLING SYSTEMS

In a practical two-phase immersion cooling system for power dense PCB based converters, several departures can be

expected from the idealised conditions imposed during boiling heat transfer experiments:

1) Components are contained in a sealed enclosure which is evacuated of air and saturated with dielectric fluid as depicted in Fig. 1(b). During converter operation, the fluid reaches an elevated saturation pressure and temperature determined by the heat flow. When the system is idle, the vapour pressure at ambient temperature is usually subatmospheric. The sealing mechanism must therefore prevent loss of fluid when pressurized and minimise leakage of air into the enclosure when idle (as this would significantly degrade performance) [24]. Despite mechanical challenges associated with system pressurisation, it could yield advantages from a thermal perspective due to increased fluid saturation temperature. Previous studies have reported moderate improvements in heat transfer coefficient and critical heat flux with increasing saturation temperature due to favourable changes in physical properties [25], [26].
2) Compact circuit layouts impose constraints on heat spreader size. It is desirable to integrate decoupling capacitors and gate drivers in close proximity to semiconductor switches on the PCB to minimise parasitic inductances and achieve the highest switching speeds and lowest switching losses [27]. A heat spreader should therefore not extend horizontally as this requires spacing out of components. However, due to the low vertical profile of the switches compared with other components like Multi-Layer Ceramic Capacitors (MLCCs), heat spreaders may extend vertically without increasing converter volume. Modelling and design of vertically protruding features like fins is complicated by the non-linear nature of boiling heat transfer.
3) The heat exchanger required to condense working fluid may not be arbitrarily large. A useful metric for comparing the *electrical* power density achievable with a particular cooling technology is the Cooling System Performance Index or CSPI [28]. It is a measure of *thermal* power density per degree of temperature rise between the switch and ambient in $\mathrm{WL^{-1}\ K^{-1}}$. Immersion cooling systems in previous literature have typically enclosed only the semiconductor switches in a dielectric fluid enclosure which is coupled to a separate commercial heat exchanger by pipe work. The following CSPI values have been estimated based on enclosure and heat exchanger volumes but not the pipe work: 19 $\mathrm{WL^{-1}\ K^{-1}}$ was achieved using an air-cooled fin tube radiator [23] and 33 $\mathrm{WL^{-1}\ K^{-1}}$ was demonstrated with a water-cooled parallel plate heat exchanger [29]. It is anticipated that systems for PCB converters will immerse the entire circuit board. This offers the advantage of a uniform temperature environment, cooling ancillary components in the circuit, and reducing hot spots on the board. Furthermore, integration of the heat exchanger and fluid enclosure could reduce converter complexity and volume by eliminating pipe work. To the authors' knowledge, only one prior study has detailed an immersion cooling system with these characteristics [30]. However, the design was intended to explore achievable switch-level heat fluxes rather than to optimise power density and demonstrated a CSPI lower than 5 $\mathrm{WL^{-1}}$ $\mathrm{K^{-1}}$.

**TABLE 1. Candidate Working Fluids and Their Thermophysical Properties**

| | **FC72** [32] | **Novec 649** [33] | **Novec 7000** [34] | **Methanol** [35] |
|---|---|---|---|---|
| Liquid thermal conductivity $k_\mathrm{l}$ ($\mathrm{W\,m^{-1}\,K^{-1}}$) | 0.056 | 0.059 | 0.075 | 0.202 |
| Specific heat capacity $c_\mathrm{p}$ ($\mathrm{J\,kg^{-1}\,K^{-1}}$) | 1100 | 1103 | 1300 | 2120 |
| Liquid dynamic viscosity $\mu_\mathrm{l}$ ($\mathrm{mPa\,s}$) | 0.640 | 0.640 | 0.450 | 0.544 |
| Latent heat $l_\mathrm{lv}$ ($\mathrm{kJ\,kg^{-1}}$) | 88 | 88 | 142 | 1165 |
| Boiling point ($^\circ\mathrm{C}$) | 56 | 49 | 34 | 65 |
| CHF $q_\mathrm{chf}$ ($\mathrm{W\,cm^{-2}}$) | 15.0 | 15.9 | 20.6 | 61.9 |

Liquid properties are at 25 °C while two-phase properties are at atmospheric pressure.

This paper aims to investigate these aspects of sealed dielectric fluid two-phase immersion cooling. The envisioned application is a PCB-based electric vehicle motor drive inverter which rejects heat to a 65 °C water glycol coolant loop (in accordance with U.K. Advanced Propulsion Centre specifications [31]). A test apparatus is detailed in Section II which represents the inverter with a realistic heat exchanger. It is employed in Section III to identify critical heat flux limits for flat switch surfaces in Novec 7000 dielectric fluid at saturation temperatures from 65 °C to 94 °C. A non-linear 1-D model of boiling heat transfer for fins is proposed in Section IV and solved numerically to design a heat spreader which increases the switch-level heat transfer coefficient by a factor of 2.3 with minimal penalty on inverter volume and electrical layout. Experiments conducted with smooth and grit-blasted fins illustrate that simple surface enhancement techniques offer substantial improvement in performance. Finally, Section V proposes a practical two-phase cooling concept featuring whole PCB immersion which is competitive with the best systems presented in previous literature.

## II. PRELIMINARIES

### A. FLUID SELECTION

In the envisioned application, the working fluid must provide electrical isolation between electronic components and the heat exchanger. Fluorinert (FC) and Novec fluids from 3 M offer high dielectric strength and are also widely chemically compatible. Important physical properties of several fluids are presented in Table 1.

Thermal conduction, convection and liquid-to-vapour phase change all contribute to high heat transfer coefficients observed during boiling. It is therefore favourable to use fluids with low viscosity, high thermal conductivity and high latent

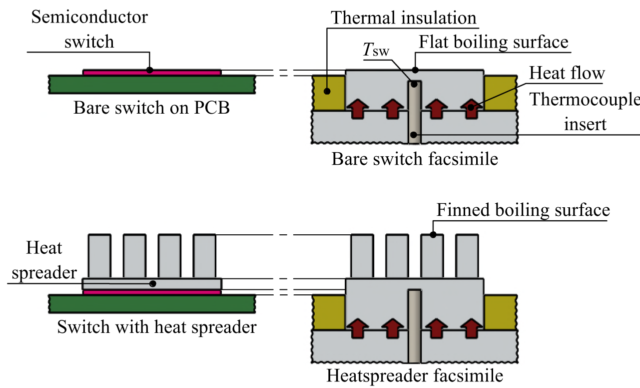


**FIGURE 3. Facsimiles used in this work to represent a bare switch and switch attached to heat spreader.**

heat. Consider the critical heat flux: mechanisms which transport vapour away from the switch surface become insufficient to contend with the rate of vapour generation. A higher latent heat reduces vapour generation for the same heat flux, resulting in a higher value of CHF. This is reflected in the widely used hydrodynamic instability model of critical heat flux shown in (3) for an infinite flat heater. It features a linear dependence of CHF on latent heat [36]:

$$q_{\mathrm{chf}} = 0.149\rho_{\mathrm{v}}^{0.5} l_{\mathrm{lv}} \sqrt[4]{g(\rho_{\mathrm{l}} - \rho_{\mathrm{v}})\sigma} \tag{3}$$

Novec 7000 was selected for its high latent heat, thermal conductivity and predicted critical heat flux at atmospheric pressure compared with other Fluorinert and Novec fluids. Organic solvents were also considered; for reference, methanol is included in Table 1. Calculation of CHF indicates an increase by a factor of 1.9 over Novec 7000. Substantial improvements in power density should be expected with methanol. However, due to practical concerns regarding chemical compatibility, only Novec 7000 was experimentally characterised.

### B. EXPERIMENTAL APPROACH

In this work, immersed semiconductor switches are represented by facsimiles machined in metal. Using this approach, the heat flow can be set using simple resistive heating elements and a thermocouple inserted close below the facsimile surface can provide measurements of the corresponding switch surface temperature $T_{\mathrm{sw}}$. As illustrated in Fig. 3, each facsimile has the same planar area exposed to fluid as the switch. All surrounding material which facilitates heat flow is thermally insulated. Two cases are considered; a bare switch facsimile with a flat boiling surface and a heat spreader facsimile representing the same switch soldered to a finned heat spreader with equal planar area. The latter case is tested with both smooth and grit-blasted surfaces.

Based on this concept, an experimental apparatus was developed to characterise the thermal performance of two-phase immersion cooling for a prospective motor drive inverter. The fluid is contained within an open-ended 52 mm outer diameter borosilicate viewing tube sealed between an aluminium heater block and heat exchanger via an arrangement of nitrile O-rings as shown in Fig. 4. The heater is machined in aluminium 6082 with six 12.6 mm × 5.6 mm facsimiles for GaN systems 650 V 150 A GS-065-150-1-D2 bare die switch. An array of pin fins is optionally machined into the facsimile surfaces; selection of the pin fin dimensions is discussed further in Section IV. Four cartridge heaters insert into the block to set the total power dissipation. A polyetheretherketone (PEEK) part fits tightly around the facsimiles, minimising heat transfer from the heater block bulk material to the fluid. The sides and base of the block are also insulated with PEEK to minimise heat loss to ambient.

The custom heat exchanger features a 43.5 mm diameter surface enhanced with pin fins on the condenser side. A Polyscience AP15R-40-A11B circulator supplies water through the liquid cooling channel at a fixed temperature set point. Unless otherwise mentioned, this was maintained at 65 °C. The flow rate is set high to maintain the temperature difference from water inlet to outlet below 10 °C. Two thermocouples are embedded in the heat exchanger to measure the temperature close to the base of the condenser fins.

A Bourns BPS130 pressure sensor is mounted on the heat exchanger via a port sealed with a nitrile O-ring. This provides measurements of the saturation pressure which can be used to estimate the bulk temperature of the fluid, provided the system is saturated with vapour and free of air.

A simple evacuation and filling procedure is followed to purge air from the experiment: The apparatus is completely filled with fluid, after which the fill port is closed off with a clip. Heat is applied and liquid boiled off to atmosphere through an evacuation port until the desired fill height is reached. The port is then closed, leaving a completely sealed system saturated with working fluid vapour. Pressure was continuously monitored over the course of several days following one fill and evacuation cycle. Once the system had cooled to room temperature, the pressure became equal to the expected fluid vapour pressure and there was negligible further change in pressure, indicating minimal leakage of air into the apparatus over timescales required to run experiments.

After evacuating and filling, power is provided via the cartridge heaters in increments. After each step in power, the system is allowed to reach steady state then ten sequential readings are made for each measured quantity and averaged. The six switch facsimile temperatures are used to calculate an *average* switch temperature $T_{\mathrm{sw}}$. The thermocouples embedded in the heat exchanger are used to estimate the temperature at the base of the condenser fins, $T_{\mathrm{b}}$. The fluid temperature $T_{\mathrm{sat}}$ is dependent on the measured pressure $P_{\mathrm{sat}}$ according to the following relationship provided by the manufacturer [34].

$$P_{\mathrm{sat}} = \exp\left(\frac{-3548.6}{T_{\mathrm{sat}} + 273.15} + 22.978\right) \tag{4}$$

Along with the main heat flow from switch facsimiles to dielectric fluid, there is a loss path to ambient air from the insulated surfaces of the heater block. To evaluate these

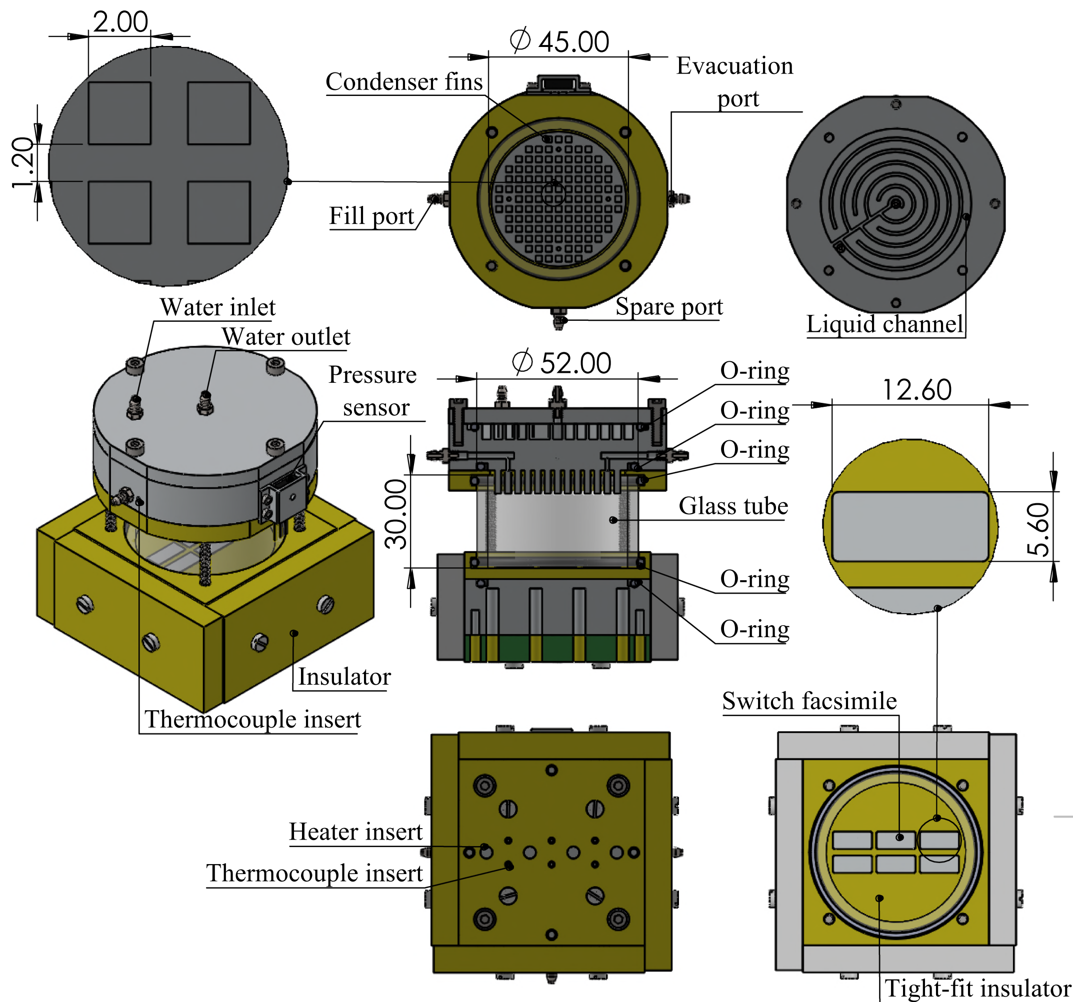


**FIGURE 4. Diagram of experimental apparatus assembly. All dimensions are in millimetres.**

losses, a calibration experiment was conducted with the heater block detached from the glass chamber/heat exchanger and the switch facsimiles covered by insulating wool. All power applied in this test was lost to ambient air through the PEEK insulation. A linear relationship was observed between the heat loss and the average facsimile temperature rise above the ambient air temperature. This relationship was used in all experiments to compensate for heat loss through the insulation. Calibration was performed separately for two different heater blocks with bare switch and finned facsimiles respectively and the observed difference between the two was negligible. Losses to ambient air account for 10% of the highest total heat reported. Further corrections were made to account for heat transfer to the fluid through the tight-fitting PEEK insulator and for resistive losses in the cartridge heater leads. These contributions were calculated to be $<2\%$ of the highest total heat.

Standard uncertainty propagation techniques were applied to calculate error bars in switch-level heat transfer coefficients and heat fluxes which are displayed on subsequent plots. The calculations incorporate uncertainties associated with the power supply, pressure sensor and thermocouples. The high relative uncertainty in heat transfer coefficient arises from the thermocouple accuracy, which was determined to be $\pm 0.5°C$ from the maximum deviation between different thermocouples measuring the same temperature.

## III. BOILING HEAT TRANSFER ON FLAT BARE SWITCH SURFACES

Fig. 5 shows photographs of the apparatus during an experiment, illustrating the boiling and condensation of the dielectric fluid. Fig. 6 shows the variation of temperatures $T_{sw}$, $T_{sat}$, $T_b$ and pressure $P_{sat}$ with power for the bare switch facsimile with 65 °C water set point. $T_{sw}$ reached 125 °C at the highest power of 182 W, beyond which critical heat flux was observed and the experiment halted. The fluid-to-switch temperature rise ($T_{sw} - T_{sat}$) just before CHF accounts for over half of the total increase above the water set point.

Fig. 7 shows the corresponding variation in switch-level heat flux with temperature difference between switch and fluid. A maximal heat flux of 43 W cm$^{-2}$ was observed. Critical heat flux was identified just beyond this point by a

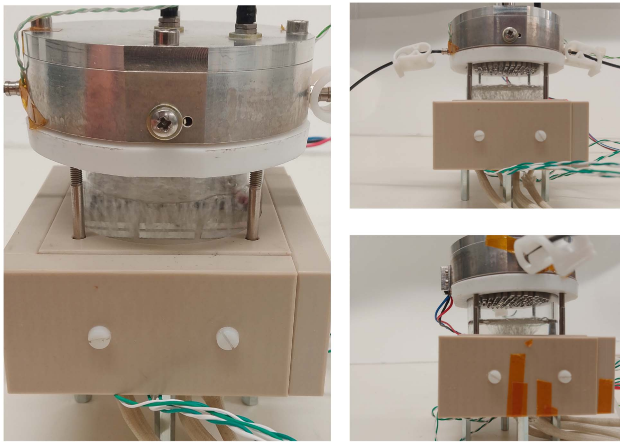

FIGURE 5. Photographs of experimental apparatus showing boiling and condensation of the dielectric fluid.

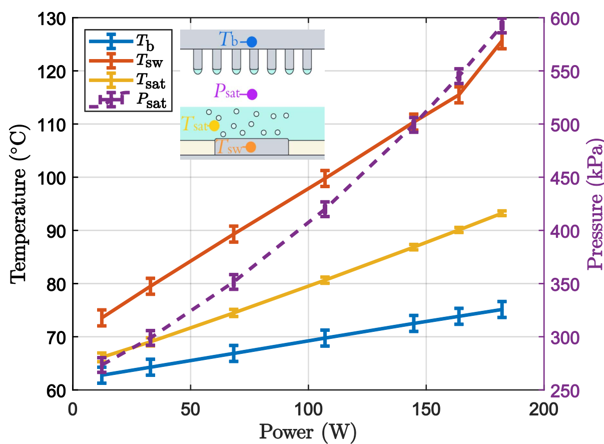


FIGURE 6. Temperatures $T_{sw}$, $T_{sat}$, $T_b$ and pressure $P_{sat}$ at varying power for the bare switch facsimile. The image illustrates physical locations of each quantity.

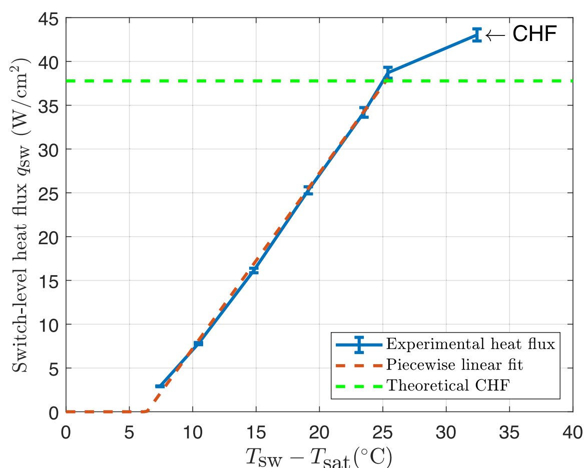


FIGURE 7. Heat flux as a function of temperature rise $T_{sw}$ - $T_{sat}$ for the bare switch facsimile.

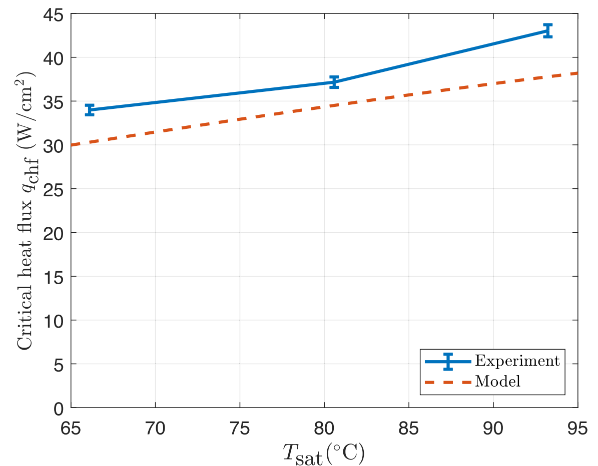


FIGURE 8. Experimental measurements and theoretical predictions of critical heat flux for a flat surface at different saturation temperatures.

rapid increase in $T_{sw}$ and an accompanying sudden decrease in pressure. The latter effect occurs as vapour blankets the switch facsimiles, instantaneously reducing heat transfer from the surface to the fluid. Since the rate of condensation is momentarily unchanged, there is a net reduction in vapour mass and hence pressure. The CHF value presented here is approximately twice that reported for Novec 7000 at atmospheric pressure. This is in accordance with observations in [25], where critical heat flux increases substantially with fluid temperature/pressure for methanol, water and pentanol. To further explore this trend, additional experiments were conducted with the water temperature set to 35 °C and 50 °C respectively, such that critical heat flux would occur at reduced fluid saturation temperatures. Fig. 8 displays the critical heat flux value as a function of fluid saturation temperature. Also shown for comparison are theoretical values derived from (3) using datasheet relations and simple thermodynamic assumptions (such as ideal gas behaviour) to model temperature dependency of physical properties. The experiment demonstrates an increase in CHF with saturation temperature in accordance with theory and agrees with the model to within 12%. The discrepancy is attributed to underestimation of the vapour density via the ideal gas model.

The experimentally observed critical heat flux has important implications for performance of a practical motor drive inverter. If the maximum allowed temperature at the switch surface is 125 °C, the resulting switch-level heat flux would be very close to CHF and the power dissipation should be reduced to prevent thermal failure.

Fig. 7 also shows a piecewise linear fit to the experimental data which is employed in Section IV to simulate heat spreaders. One line segment is obtained using least-squares regression on the data, yielding the following relationship between the heat flux $q_{sw}$ and temperature difference $T_{sw}$ −

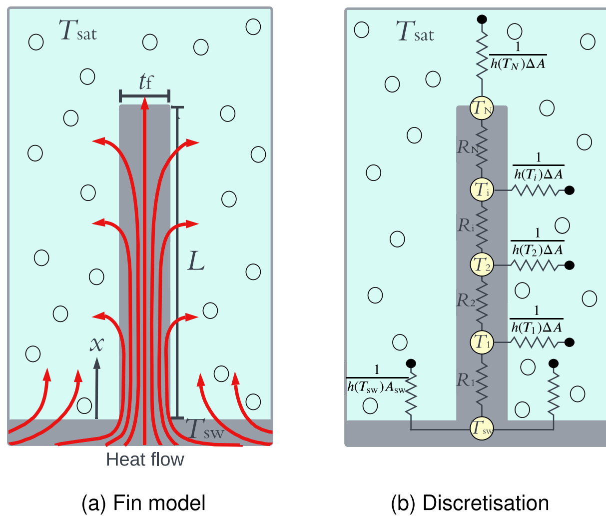


**FIGURE 9.** Diagrams depicting boiling heat transfer from the surface of an immersed fin and discretisation of the fin for numerical solving.

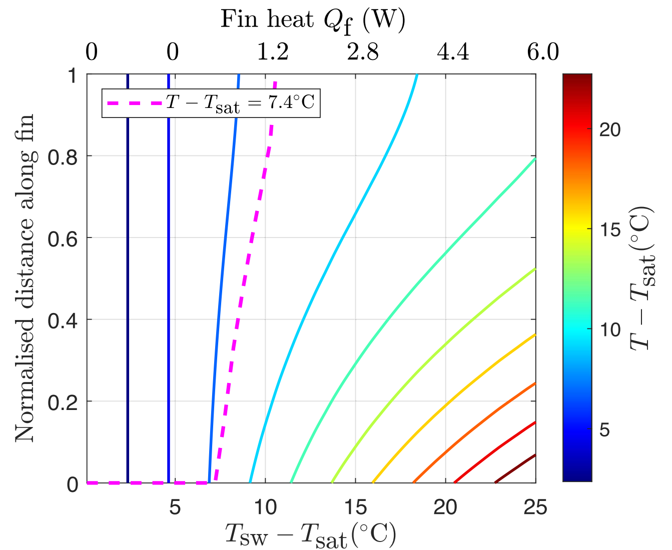


**FIGURE 10.** Contours showing temperature variation along selected fin for varying $T_{sw} - T_{sat}$.

$T_{sat}$:

$$q_{sw} = 2.0(T_{sw} - T_{sat}) - 12.8 \tag{5}$$

For zero temperature difference, (5) predicts a negative heat flux which contradicts the expectation of zero heat transfer. This is because it does not accurately model fluid behaviour at low heat fluxes, where a transition from natural convection to nucleate boiling occurs. In the absence of experimental data for this region, it is assumed the heat flux is zero between the origin and the intercept of (5) with the x-axis.

The proposed piecewise linear model does not incorporate dependence of fluid physical properties on saturation temperature. By varying the flow side water temperature from 35 °C to 65 °C, the maximum heat transfer coefficient increased by only 11% as the corresponding fluid saturation temperature rose from 66 °C to 94 °C. This justifies the model assumption that heat flux is senstive only to the temperature difference $T_{sw} - T_{sat}$.

## IV. BOILING HEAT TRANSFER ON FINNED HEAT SPREADER SURFACES

Heat spreaders reduce switch operating temperature for the same converter power dissipation and eliminate the risk of critical heat flux. Due to constraints imposed by printed circuit board substrates, the heat spreader considered in this work has the same planar area as the switch and incorporates vertically protruding fins to increase the heat transfer area.

### A. THEORETICAL MODEL

Fig. 9(a) depicts a square pin fin of length $L$ and width $t_f$ immersed in a pool of dielectric liquid at saturation temperature $T_{sat}$. The fin material has thermal conductivity $k$ and boiling is modelled as a temperature dependent heat transfer coefficient $h(T)$. In steady-state, the temperature $T$ some distance $x$ along the fin is given by the one dimensional heat equation below [9].

$$k\frac{d^2T}{dx^2} = \frac{4h(T)}{t_f}(T - T_{sat}) \tag{6}$$

A constant switch temperature $T_{sw}$ is applied at the fin base and the following heat transfer coefficient boundary condition is assumed at the fin tip.

$$-k\left.\frac{dT}{dx}\right|_{x=L} = h(T|_{x=L})(T|_{x=L} - T_{sat}) \tag{7}$$

In this work, as in previous literature [19], it is assumed the heat transfer coefficient along the fin sides is independent of orientation and equal to that for an isothermal flat surface at the same temperature. It can therefore be obtained via (2) using the piecewise linear fit for heat flux from Section III and substituting the *fin* temperature $T$ in place of $T_{sw}$. The problem is solved numerically by discretising (6) and (7) using a finite difference approximation for the derivatives. This is illustrated conceptually in Fig. 9(b). The fin is divided into $N$ nodes with temperature $T_i$ and local heat transfer coefficient $h(T_i)$ (represented by an equivalent thermal resistance for an incremental area $\Delta A$). Heat conduction between two adjacent nodes is represented by the connecting thermal resistance $R_i$. The heat transfer $Q_f$ through a single fin is evaluated using Fourier's law at the base, yielding (8). The total power for a heat spreader is obtained by summing for all fins and adding a contribution from the heat spreader base.

$$Q_f = -kt_f^2\left.\frac{dT}{dx}\right|_{x=0} \tag{8}$$

Fig. 10 depicts contours showing dependence of temperature on distance along the chosen fin (normalised to its length) for varying temperature difference between the fin base and the fluid ($T_{sw} - T_{sat}$). The corresponding variation in fin heat

transfer $Q_f$ is also shown. The chosen heat spreader design features eight such fins; for the highest experimental switch power dissipation of 31 W in this work, the per-fin heat transfer is therefore approximately 3.9 W.

The piecewise linear model can not accurately represent fluid behaviour when the fin is < 7.4°C hotter than the fluid saturation temperature due to lack of experimental data in this region. The dotted contour on Fig. 10 represents the fin height above which this occurs. As the fin base temperature increases from 8 °C to 11 °C above the fluid saturation temperature, the portion of the fin for which $T - T_{sat} < 7.4$°C diminishes to zero. Beyond this, the model is expected to accurately predict fluid behaviour along the entire fin.

At the highest value of $T_{sw} - T_{sat}$ shown in Fig. 10, the temperature difference along the fin accounts for 14 °C of the 25 °C rise at the fin base, leading to a corresponding reduction in heat transfer coefficient by a factor of 2.3 from base to tip. This emphasizes the importance of incorporating heat transfer dependence on temperature in contrast to using analytical models with a constant heat transfer coefficient.

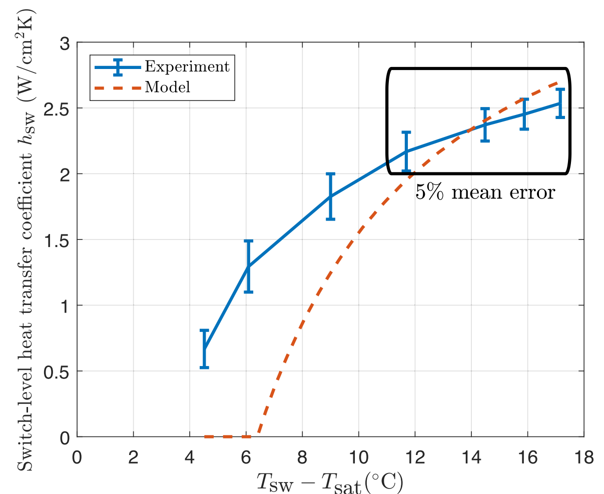


**FIGURE 11.** **Comparison between experimental switch-level heat transfer coefficients for smooth heat spreader facsimiles and theoretical values calculated using the numerical fin model.**

### B. EXPERIMENTAL RESULTS

A modified heater block was manufactured with six heat spreader facsimiles, each enhanced with a regular array of pin fins. Due to technological constraints of the CNC milling process used, the spacing between fins could be no smaller than 1 mm. Imposing a minimum spacing is also advantageous from a thermal point of view as it minimises the risk of vapour coalescence in the gaps [19]. The proposed model was solved for different fin arrangements and the best performance was predicted for eight fins of width 2 mm. A fin length of 4 mm was selected by considering the largest 650 V surface mount MLCC in 2220 footprint which has height of 5.4 mm. Therefore a heat spreader with 4 mm fins and 1 mm thick base could be attached to the 0.3 mm thick switch with no penalty on converter power density.

The same experimental procedure was followed for the modified heater block as in Section III, up to a total power of 186 W and a corresponding switch-level heat flux of 44 W cm$^{-2}$. Higher power dissipations were not tested due to restrictions on the pressure capability of the borosilicate enclosure. The maximum average switch temperature reached was 110 °C. This is 15 °C cooler than the bare switch facsimile at the same heat power. Fig. 11 compares experimental switch-level heat transfer coefficients with theoretical values predicted by the model from Section IV-A. The model significantly underestimates the first three datapoints due to the pessimistic assumption of zero heat flux in the natural convection regime. However, the mean percentage error is 5% when only the last four data points are considered, for which the simulation in Fig. 10 predicts the entire fin is over 7.4 °C hotter than the fluid. This demonstrates the usefulness of simple fin heat transfer models with flat surface boiling data as a tool for predicting heat spreader performance without requiring complex simulations of fluid behaviour or experimental characterisation of each fin arrangement.

The heat spreader facsimile does not exhibit critical heat flux within the power range surveyed. Another test was conducted with five of the six facsimiles covered by tight-fitting PEEK caps in an effort to induce CHF. An apparent switch-level heat flux of 130 W cm$^{-2}$ was sustained through the single exposed facsimile with no indication of CHF. By calculating the fin heat transfer when the spreader base reaches critical heat flux through (3), an expected value of 108 W cm$^{-2}$ was obtained. The discrepancy between model and experiment is likely due to heat transfer from the covered facsimiles, which could not be completely eliminated.

In a further step, the heat spreader facsimile surfaces were grit-blasted to favourably influence their surface microgeometry. The experiment was repeated up to 186 W and 44 W cm$^{-2}$; the measured heat transfer coefficients for all three tests (flat surface, smooth fins, grit-blasted fins) are shown in Fig. 12. The maximum heat transfer coefficient increased from 1.5 W m$^{-2}$ K$^{-1}$ to 2.5 W m$^{-2}$ K$^{-1}$ by incorporating fins, further improving to 3.4 W m$^{-2}$ K$^{-1}$ by grit blasting. Notably, this performance is achieved using a relatively low conductivity spreader material (aluminium 6082 alloy, 170 W m$^{-1}$ K$^{-1}$), a simple surface enhancement technique, and with negligible impact on the electrical layout and power density of a prospective converter.

## V. IMMERSION-COOLED PCB CONVERTERS

Fig. 13 depicts a practical two-phase immersion cooling concept for a PCB based motor drive inverter. It features two fluid enclosures which seal to top and bottom of the circuit board respectively. This allows for cut-outs/vias in the design and provides pressure equalisation between the two sides. A portion of the circuit board extends beyond the enclosure walls so connections can be made via the power terminals. The heat exchanger is integrated into the top side chamber. The condenser side of the heat exchanger features downward

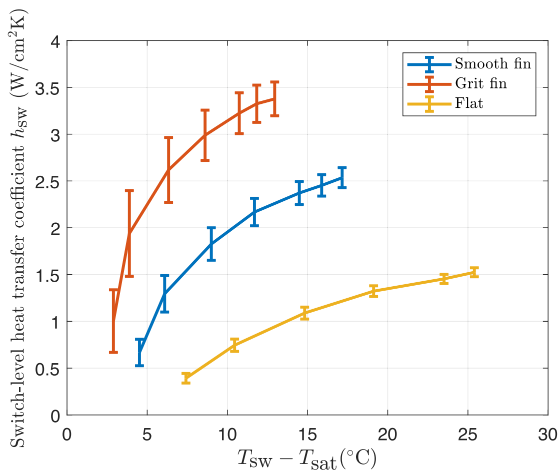


**FIGURE 12.** Experimental switch-level heat transfer coefficients for flat surface, smooth fins and grit-blasted fins.

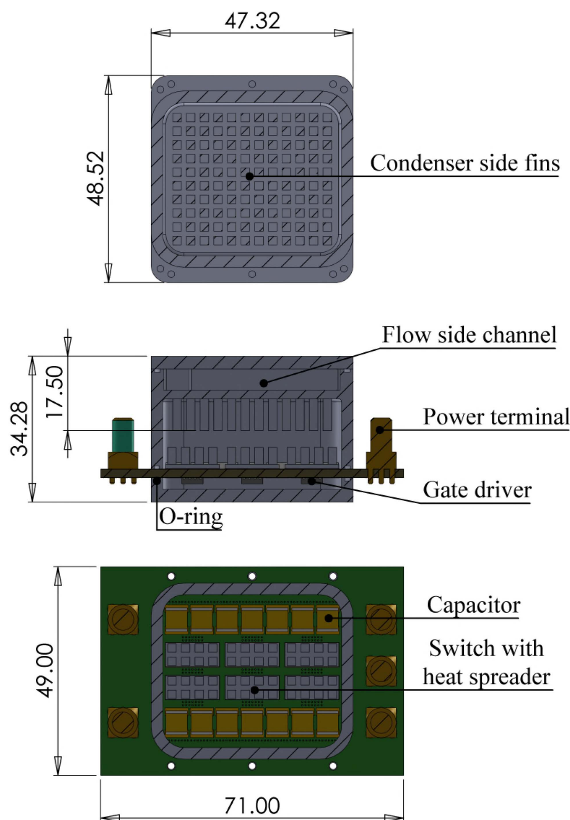


**FIGURE 13.** Proposed PCB layout and integrated fluid enclosure/heat exchanger for an immersion cooled EV motor drive.

facing fins to increase surface area and promote gravity-driven return of condensate while the flow side features channels for pumped liquid coolant.

The PCB comprises six 650 V GaN Systems GS-065-150-1-D2 bare die switches and 14 2220 footprint multi-layer ceramic capacitors on the top side. The largest 650 V capacitor in this package has capacitance 0.2 $\mu$F, yielding a total decoupling capacitance of 2.8 $\mu$F. This is over 500 times larger than the combined output capacitance of all six switches (800 pF each [37]). In previous literature, a ratio of 50 was deemed sufficient [38]. The bottom side of the printed circuit board is populated by gate drive circuitry.

The heat exchanger condenser side and the heat spreaders have the same fin arrangements as the experimental apparatus so the thermal performance is comparable. Assuming the heat spreaders are grit-blasted, a power dissipation of 186 W would yield a switch temperature of 107 °C. This is well below the rated junction temperature of 150 °C and allows for additional thermal resistance associated with the bond between switch and heat spreader. The switch-level heat flux is 44 W cm$^{-2}$, less than half of the predicted critical heat flux for the heat spreader facsimile in Section IV-B.

The system volume is 0.12 L including PCB converter, power terminals, heat exchanger and the additional enclosure on the board underside. The resulting CSPI is 37 W L$^{-1}$ K$^{-1}$. For comparison, a conceptually similar system featuring PCB-mounted test cells in an aluminium enclosure filled with Novec 649 dielectric fluid was demonstrated in [30]. Based on the reported thermal performance and the enclosure volume, a CSPI of 4.4 W L$^{-1}$ K$^{-1}$ was achieved. Some authors have reported substantially higher CSPI values by using pumped fluid techniques such as microchannels or impinging jets in direct contact with semiconductor switches [5]. However, these studies typically do not incorporate the volume occupied by the pump or liquid-to-liquid heat exchanger which rejects heat to the main water-glycol loop. Furthermore, electrical isolation between the switches and cooling system is often not considered; in this work it is provided by the dielectric fluid.

Neglecting the capacitors and gate drivers, the total inverter power dissipation can be equated to the sum of conduction and switching losses for semiconductor switches. Owing to the fast switching transitions of GaN devices, it can be assumed switching losses are negligible at frequencies used for motor drives. Given the switch on-state resistance of 14 m $\Omega$ at 150 °C, the maximum RMS motor phase current is 66 A. A three phase inverter using third harmonic injection can deliver an RMS line-to-line voltage of 490 V from a 400 V DC bus, this yields an apparent power rating of 33 kV A. The resulting power density is 280 kW/L, demonstrating the potential of two-phase immersion to produce high power density converters on printed circuit boards.

Tests were conducted to explore robustness of the proposed immersion cooling concept to air leakage. An experimental apparatus was constructed with two aluminium fluid enclosures sealing to a printed circuit board via elastomer O-rings. Several thermal cycles were undertaken over the duration of a month in which power was periodically applied to heat up the dielectric fluid. No changes were observed in both the positive pressure reached during heating and the sub-atmospheric pressure when idle. This suggests negligible air leakage over one-month timescales, though more comprehensive tests are required to draw conclusions concerning performance degradation over a typical converter lifetime of many years.

## VI. CONCLUSION

A sealed two-phase immersion cooling concept for an electric vehicle motor drive inverter on a single PCB was presented. Experiments conducted with a representative mechanical apparatus indicate the critical heat flux limit for boiling on a planar switch surface increases from 20 W $cm^{-2}$ at the atmospheric pressure boiling point of 34 °C to 43 W $cm^{-2}$ at a saturation temperature of 94 °C and pressure of 593 kPa. This result agrees well with theoretical predictions and can be attributed to favourable changes in fluid physical properties.

A non-linear 1-D heat transfer model for boiling on fin surfaces was detailed and used to design a heat spreader which significantly improves thermal performance with minimal penalty on the converter electrical layout and size. The model demonstrates reasonable agreement with experimental switch-level heat transfer coefficients which are as high as 2.5 W $m^{-2}$ $K^{-1}$ (compared with 1.5 W $m^{-2}$ $K^{-1}$ for a planar surface). Grit blasting of the fins yielded further improvement to 3.4 W $cm^{-2}$ $K^{-1}$. This illustrates that appropriately sized heat spreaders can be used to reduce the switch temperature for the same power dissipation and mitigate the risk of critical heat flux.

To evaluate the potential CSPI of this approach a PCB-based motor drive was designed. To the authors' knowledge, the CSPI value of 37 $WL^{-1}$ $K^{-1}$ is competitive with the best solutions using separate commercial heat exchangers with the unique advantage of close component integration on a single PCB.

Future research could investigate the reliability of sealing systems for two-phase immersion cooling over long time scales.

## ACKNOWLEDGMENT

The authors thank Simon Hart, Dan Rendell, Paul Spendley, Rajesh Kudikala and Tony Webster of YASA Ltd. for their advice on technical matters.

## REFERENCES

[1] S. M. I. Rahman et al., "Emerging trends and challenges in thermal management of power electronic converters: A state of the art review," *IEEE Access*, vol. 12, pp. 50633–50672, 2024.
[2] G. Moreno, S. Narumanchi, J. Tomerlin, and J. Major, "Single-phase dielectric fluid thermal management for power-dense automotive power electronics," *IEEE Trans. Power Electron.*, vol. 37, no. 10, pp. 12474–12485, Oct. 2022.
[3] G. Tang, L. C. Wai, and H. Feng, "Development and demonstration of a novel immersion two phase cooling high power SiC power module," in *Proc. IEEE 2023 73rd Electron. Compon. Technol. Conf.*, 2023, pp. 1553–1558.
[4] B. Tian, W. Chang, E. Santi, C. Li, T. Zhang, and L. Yuan, "Two-phase milli/microchannel cooling for SiC power module using dielectric fluid coolant," in *Proc. IEEE 2021 Electric Ship Technol. Symp.*, 2021, pp. 1–7.
[5] S. U. Yuruker, R. K. Mandel, P. McCluskey, and M. Ohadi, "A vertically enhanced manifold microchannel system for thermal management of power electronics," *IEEE Trans. Compon. Packag. Manuf. Technol.*, vol. 11, no. 10, pp. 1716–1723, Oct. 2021.
[6] P.-Y. Lin, S.-L. Kuo, K. Yan, W.-M. Chen, and M. D. -D. Liao, "Advanced thermal integration for HPC packages with two-phase immersion cooling," in *Proc. IEEE 2022 72nd Electron. Compon. Technol. Conf.*, 2022, pp. 566–573.
[7] Y. Wang, L. Ren, Z. Yang, Z. Deng, and W. Ding, "Application of two-phase immersion cooling technique for performance improvement of high power and high repetition avalanche transistorized subnanosecond pulse generators," *IEEE Trans. Power Electron.*, vol. 37, no. 3, pp. 3024–3039, Mar. 2022.
[8] P. Birbarah et al., "Water immersion cooling of high power density electronics," *Int. J. Heat Mass Transfer*, vol. 147, 2020, Art. no. 118918, [Online]. Available: https://www.sciencedirect.com/science/article/pii/S0017931019336002
[9] A. Bejan and A. D. Kraus, *A Heat Transfer Handbook*. Hoboken, NJ, USA: Wiley, 2003.
[10] S. Nukiyama, "The maximum and minimum values of the heat Q transmitted from metal to boiling water under atmospheric pressure," *Int. J. Heat Mass Transfer*, vol. 9, no. 12, pp. 1419–1433, 1966. [Online]. Available: https://www.sciencedirect.com/science/article/pii/0017931066901384
[11] T. M. Anderson and I. Mudawar, "Microelectronic cooling by enhanced pool boiling of a dielectric fluorocarbon liquid," *J. Heat Transfer*, vol. 111, no. 3, pp. 752–759, Aug. 1989, doi: 10.1115/1.3250747.
[12] M. S. El-Genk and M. Pourghasemi, "Experimental investigation of saturation boiling of HFE-7000 dielectric liquid on rough copper surfaces," *Thermal Sci. Eng. Prog.*, vol. 15, 2020, Art. no. 100428. [Online]. Available: https://www.sciencedirect.com/science/article/pii/S2451904919302343
[13] O. Ghaffari, F. Grenier, J.-F. Morissette, M. Bolduc, S. Jasmin, and J. Sylvestre, "Pool boiling experiment of dielectric liquids and numerical study for cooling a microprocessor," in *Proc. IEEE 2019 18th Intersociety Conf. Thermal Thermomechanical Phenomena Electron. Syst.*, 2019, pp. 540–545.
[14] M. S. El-Genk, "Nucleate boiling enhancements on porous graphite and microporous and macrofinned copper surfaces," *Heat Transfer Eng.*, vol. 33, no. 3, pp. 175–204, 2012, doi: 10.1080/01457632.2011.589305.
[15] C. Falsetti, J. Chetwynd-Chatwin, and E. J. Walsh, "Pool boiling heat transfer of novec 649 on sandblasted surfaces," *Int. J. Thermofluids*, vol. 22, 2024, Art. no. 100615. [Online]. Available: https://www.sciencedirect.com/science/article/pii/S2666202724000570
[16] P. E. Tuma, "Evaporator/boiler design for thermosyphons utilizing segregated hydrofluoroether working fluids," in *Proc. IEEE 22nd Annu. Semicond. Thermal Meas. Manage. Symp.*, 2006, pp. 69–77.
[17] K. J. L. Geisler and A. Bar-Cohen, "Optimization of pool boiling heat sinks including the effects of confinement in the interfin spaces," *J. Electron. Packag.*, vol. 130, no. 4, Nov. 2008, Art. no. 041002, doi: 10.1115/1.2993135.
[18] S. J. Reed and I. Mudawar, "Enhancement of boiling heat transfer using highly wetting liquids with pressed-on fins at low contact forces," *Int. J. Heat Mass Transfer*, vol. 40, no. 10, pp. 2379–2392, 1997. [Online]. Available: https://www.sciencedirect.com/science/article/pii/S0017931096002864
[19] I. Mudawar and T. M. Anderson, "Optimization of enhanced surfaces for high flux chip cooling by pool boiling," *J. Electron. Packag.*, vol. 115, no. 1, pp. 89–100, Mar. 1993, doi: 10.1115/1.2909306.
[20] J. Gess et al., "Impact of surface enhancements upon boiling heat transfer in a liquid immersion cooled high performance small form factor server model," in *Proc. IEEE 14th Intersociety Conf. Thermal Thermomechanical Phenomena Electron. Syst.*, 2014, pp. 435–443.
[21] D. Tanaka et al., "Heat transfer enhancement in two-phase immersion cooling with FC-72," in *Proc. IEEE 2023 Int. Conf. Electron. Packag.*, 2023, pp. 179–180.
[22] C. M. Barnes and P. E. Tuma, "Immersion cooling of power electronics in segregated hydrofluoroether liquids," in *Proc. Heat Transfer Summer Conf.*, Aug. 2008, pp. 719–725, doi: 10.1115/HT2008-56230.
[23] C. M. Barnes and P. E. Tuma, "Practical considerations relating to immersion cooling of power electronics in traction systems," *IEEE Trans. Power Electron.*, vol. 25, no. 9, pp. 2478–2485, 2010.
[24] P. E. Tuma, "Design considerations relating to non-thermal aspects of passive 2-phase immersion cooling," in *Proc. IEEE 2011 27th Annu. Semicond. Thermal Meas. Manage. Symp.*, 2011, pp. 1–9.
[25] W. Bailey, E. Young, C. Beduz, and Y. Yang, "Pool boiling study on candidature of pentane, methanol and water for near room temperature cooling," in *Proc. IEEE Thermal Thermomechanical 10th Intersociety Conf. Phenomena Electron. Syst.*, 2006, pp. 599–603.

[26] I. Mudawar and T. M. Anderson, "Parametric investigation into the effects of pressure, subcooling, surface augmentation and choice of coolant on pool boiling in the design of cooling systems for high-power-density electronic chips," *J. Electron. Packag.*, vol. 112, no. 4, pp. 375–382, Dec. 1990, doi: 10.1115/1.2904392.

[27] X. Tian et al., "PCB-on-DBC GAN power module design with high-density integration and double-sided cooling," *IEEE Trans. Power Electron.*, vol. 39, no. 1, pp. 507–516, Jan. 2024.

[28] U. Drofenik, G. Laimer, and J. W. Kolar, "Theoretical converter power density limits for forced convection cooling," in *Proc. Official Int. Conf. Power Electron., Intell. Motion*, 2005, pp. 608–619.

[29] F. Agostini and B. Agostini, "Flexible two-phase thermosyphon for power electronic cooling," in *Proc. IEEE 2011 33rd Int. Telecommun. Energy Conf.*, 2011, pp. 1–6.

[30] J. L. Gess, S. H. Bhavnani, and R. W. Johnson, "Experimental investigation of a direct liquid immersion cooled prototype for high performance electronic systems," *IEEE Trans. Compon. Packag. Manuf. Technol.*, vol. 5, no. 10, pp. 1451–1464, Oct. 2015.

[31] *Power Electronics Roadmap 2020 Narrative Report*, Advanced Propulsion Centre U.K., Feb. 2021. [Online]. Available: apcuk.co.uk/power-electronics-roadmap/

[32] 3M, "3M Fluorinert Electronic Liquid FC-72," *FC72 Datasheet*, Sep. 2019.

[33] 3M, "3M novec 649 engineered fluid," *Novec 649 datasheet*, Sep. 2009.

[34] 3M, "3M novec 7000 engineered fluid," *Novec 7000 datasheet*, Sep. 2021.

[35] Methanol Institute, "Physical properties of pure methanol," *Methanol datasheet*, Jun. 2016.

[36] J. H. Lienhard and V. K. Dhir, "Hydrodynamic prediction of peak pool-boiling heat fluxes from finite bodies," *J. Heat Transfer- Trans. Asme*, vol. 95, pp. 152–158, 1973. [Online]. Available: https://api.semanticscholar.org/CorpusID:120647310

[37] GaN Systems, "GS-EVx-3PH-650V300A-SM1x 650V 300A 3-Phase GaN power module external driver board evaluation kit technical manual," *GS-EVx-3PH-650V300A-SM1x datasheet*, Jun. 2021.

[38] Z. Chen, D. Boroyevich, P. Mattavelli, and K. Ngo, "A frequency-domain study on the effect of DC-link decoupling capacitors," in *Proc. IEEE 2013 Energy Convers. Congr. Expo.*, 2013, pp. 1886–1893.